Clinical Evaluation of a New Concept: Resting Myocardial Perfusion Heterogeneity Quantified by Markovian Analysis of PET Identifies Coronary Microvascular Dysfunction and Early Atherosclerosis in 1,034 Subjects

Nils P. Johnson, MD[1]; and K. Lance Gould, MD[2]

[1]*Department of Medicine, Feinberg School of Medicine, Northwestern University, Chicago, Illinois; and* [2]*Division of Cardiology, Department of Medicine, The Weatherhead PET Center for Preventing and Reversing Atherosclerosis, University of Texas Medical School at Houston and the Memorial Hermann Hospital, Houston, Texas*

Coronary endothelial dysfunction is an early marker of coronary artery disease (CAD) but its noninvasive assessment is limited. We tested the hypothesis that diffuse patchy heterogeneous resting myocardial perfusion by noninvasive cardiac PET, quantified objectively by Markovian homogeneity analysis, or its improvement during dipyridamole stress, is a predictor of even mild stress perfusion abnormalities, consistent with coronary microvascular dysfunction as an early marker of CAD. **Methods:** Rest-dipyridamole PET with ^{82}Rb was performed on 1,034 consecutive subjects for possible CAD or follow-up, for second opinion on revascularization procedures, or for screening because of risk factors and on 50 healthy control subjects. Objective, automated software quantified myocardial PET perfusion images for (i) patchy diffuse perfusion heterogeneity by Markovian homogeneity analysis separately from, independently of, and around significant localized regional perfusion defects; (ii) size and severity of localized regional perfusion defects caused by flow-limiting stenosis; and (iii) the graded base-to-apex longitudinal perfusion gradient due to early diffuse CAD without flow-limiting stenosis. History of vascular risk factors was obtained for all subjects. **Results:** Resting myocardial perfusion heterogeneity with a homogeneity index outside 1 SD of healthy reference subjects and its improvement with dipyridamole correlated closely with CAD documented by stress-induced regional myocardial perfusion abnormalities outside 1 SD independently of other risk factors by multivariate logistic regression analysis ($P < 0.001$), by multivariate linear regression analysis ($P < 0.001$), and by χ^2 analysis ($P < 0.001$). The relative odds ratios of having stress-induced myocardial perfusion abnormalities for a resting homogeneity index outside 1 SD of healthy reference subjects was highly predictive and substantially greater than for standard risk factors. **Conclusion:** Patchy heterogeneous resting myocardial perfusion by noninvasive cardiac PET quantified objectively using Markovian homogeneity analysis, and its improvement after dipyridamole, are powerful independent predictors of even mild stress-induced perfusion abnormalities, more than standard risk factors, consistent with coronary microvascular dysfunction as an early marker of preclinical CAD for potential preventive treatment.

Key Words: myocardial perfusion; PET; coronary artery disease; heterogeneity; homogeneity; microvascular function; risk factors

J Nucl Med 2005; 46:1427–1437

Coronary endothelial dysfunction is closely associated with microvascular dysfunction and coronary artery disease (CAD) or its risk factors (*1*), may be familial as an independent risk factor (*2*), and predicts future coronary events (*3–6*) or clinically manifest disease up to 10 y later (*6*). The 3 principal methods for assessing coronary endothelial function reflect different aspects of its complex multifaceted behavior with specific limitations in clinical application. The most established method using intracoronary acetylcholine requires coronary arteriography and provides information only on epicardial coronary arteries, not endothelial function of the microvasculature that is an essential component of preclinical coronary atherosclerosis. Forearm arterial vasodilation during reactive hyperemia by ultrasound is noninvasive but does not correlate specifically with coronary endothelial dysfunction (*7*). Cold pressor testing with measurements of coronary flow reserve involves complex sensory and efferent vasomotor control mechanisms separately from endothelial function with such great variability in healthy subjects that its diagnostic utility is limited (*8,9*).

The hallmark of coronary endothelial dysfunction is mild heterogeneous vasoconstriction of coronary arteries or coronary microvasculature under a wide spectrum of different

Received Dec. 19, 2004; revision accepted May 18, 2005.

For correspondence or reprints contact: K. Lance Gould, MD, The Weatherhead PET Center, University of Texas Medical School, Room 4.256MSB, 6431 Fannin St., Houston, TX 77030.

E-mail: gould@pet.med.uth.tmc.edu

conditions and vasomotor stimuli involving many different mechanisms, including inhibition of vasodilator mechanisms or activation of vasoconstrictor mechanisms by many different interacting vasoactive mediators. Heterogeneity of coronary endothelial function has been well documented in humans (*10–12*) with associated altered coronary blood flow or perfusion reflecting coronary arteriolar as well as epicardial arterial endothelial dysfunction (*13–17*). Resting coronary flow falls by approximately 20% after inhibition of coronary endothelial nitric oxide production without significant reduction in maximum coronary flow or coronary flow reserve (*18–22*), thereby reflecting altered resting microvascular function.

Therefore, we have hypothesized that the visually apparent heterogeneity of resting myocardial perfusion or its improvement after dipyridamole stress on high-quality, noninvasive PET images outside the limits of healthy control subjects is one manifestation of coronary microvascular dysfunction associated with endothelial dysfunction (*23*). Testing this hypothesis is important because coronary endothelial dysfunction is associated with early preclinical coronary atherosclerosis, increased coronary events (*3,4*), and subsequent clinically manifest CAD many years later (*6*), thereby providing a basis for intense, lifelong, pharmacologic preventive treatment.

Coronary flow reserve and myocardial perfusion imaging after pharmacologic arteriolar vasodilation for identifying flow-limiting coronary artery stenosis as first reported from this laboratory (*24–27*) is now widespread as a routine clinical diagnostic procedure. In this paradigm, the resting perfusion image serves as a baseline for comparison with the stress perfusion image for identifying discrete regional perfusion abnormalities due to flow-limiting coronary artery stenosis, myocardial scar, or hibernating myocardium. However, the current report analyzes and quantifies the distinctly different diffuse patchy heterogeneity of resting myocardial perfusion as a marker of coronary endothelial dysfunction associated with coronary atherosclerosis, independently from and around these traditional discrete regional myocardial perfusion defects caused by flow-limiting stenosis or myocardial scar.

In this study, we use a mathematic technique from Markovian homogeneity analysis (*28*) to provide precise, objective, automated quantification of resting perfusion heterogeneity in 1,034 subjects, its normal limits in 50 healthy reference subjects, and its close association with documented CAD, thereby demonstrating a basic new observation in myocardial perfusion imaging with important clinical implications.

MATERIALS AND METHODS

Study Patients

The population for this study consists of 1,034 consecutive subjects undergoing diagnostic, rest-dipyridamole, myocardial perfusion PET at The Weatherhead PET Center For Preventing and Reversing Atherosclerosis of the University of Texas Medical School–Houston. All subjects signed informed consent approved by the Committee for the Protection of Human Subjects of the University of Texas Health Science Center. A complete medical history was obtained on all patients undergoing diagnostic cardiac PET for assessment or follow-up of known CAD, for second opinions on revascularization procedures, for prior positive stress tests, for coronary calcification by CT, for chest pain or other symptoms, for screening, or for risk factors. A history of risk factors was obtained for age, sex, diabetes, hypertension, high cholesterol, family history of vascular disease, excess weight, lack of exercise, and past or present smoking, that were counted as positive even if treated, as with hypertensive or lipid-lowering medications.

PET

Patients were instructed to fast for 4 h and abstain from caffeine, theophylline, and cigarettes for 24 h before study. As previously described (*29–33*), PET was performed using the University of Texas designed, Positron Posicam Auricle, bismuth germanate, 2-dimensional (2D) multislice tomograph with a reconstructed resolution of 10-mm full width at half maximum. Using a rotating rod source containing 148–185 MBq (4–5 mCi) of ^{68}Ge, transmission images to correct for photon attenuation contained approximately 40–60 million counts. Emission images obtained after intravenous injection of 925–1,850 MBq (25–50 mCi) of generator-produced ^{82}Rb contained 20–50 million counts depending on the age of the generator and size of the patient. After resting ^{82}Rb data acquisition, dipyridamole (0.142 mg/kg/min) was infused for 4 min. At 4 min after completion of the dipyridamole infusion, the same dose of ^{82}Rb was given intravenously.

Automated Quantitative Analysis of PET Images

Completely automated analysis of the severity and size of PET abnormalities was performed by previously described software (*29–33*). A 3-dimensional (3D) restructuring algorithm generates true short- and long-axis views from PET transaxial cardiac images acquired in 2D tomographic mode to minimize scatter. From circumferential profiles, 3D topographic views of the left ventricle are reconstructed showing relative regional activity distribution divided into lateral, inferior, septal, and anterior quadrant views of the 3D topographic display corresponding to the coronary arteries illustrated in Figure 1.

Each topographic map consists of 21 slices along the long axis of the left ventricle. Every long-axis slice contains 64 radial pixels, representing equal angles around a circle (360° divided over 64 pixels equals just under 6° per pixel). The 4 quadrant views contain 16 radial pixels each. Therefore, the absolute pixel size is N-by-M, where N is 1/21 of the base-to-apex distance (different for every patient) and M is 360°/64° (same for every patient).

Activity is normalized to the maximum 2% of pixels in the whole heart dataset. Regions of each quadrant are identified as outside 97.5% confidence intervals (CI) or 2.5 SD of 50 healthy control subjects with no risk factors by complete medical history. The percentage of circumferential profile units outside 97.5% CI is calculated automatically after correcting for any misregistration of attenuation and emission images that commonly cause artifactual defects (*34*).

Markovian Homogeneity Analysis. Markovian texture or homogeneity analysis characterizes an image by examining the probability that a pixel with a given intensity will have a neighbor with a different intensity (*28*), where Pd(m) is the probability that 2 adjacent pixels have intensity values that differ by m. For this

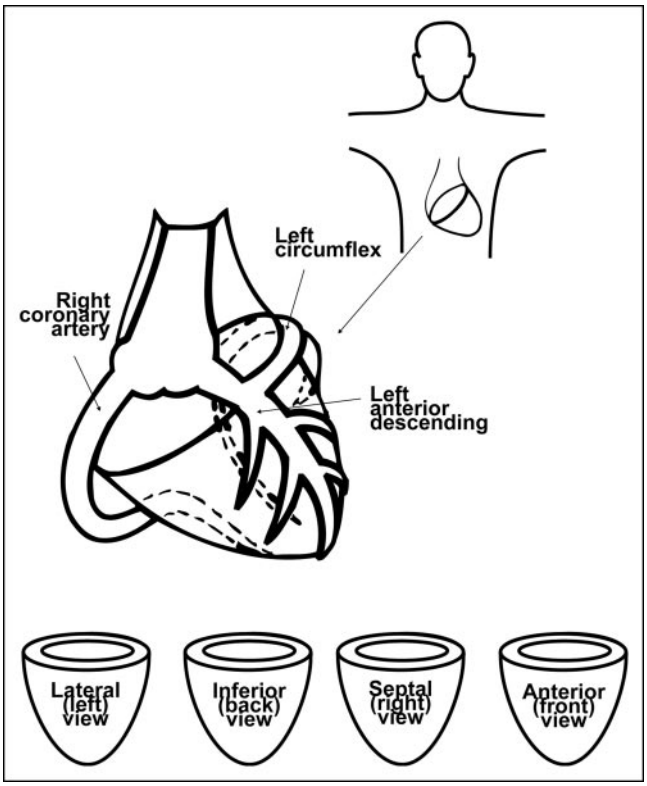

FIGURE 1. Schematic demonstrates 4 topographic views of myocardial perfusion by PET. From left to right, views are left lateral, inferior, right or septal, and anterior. Each view corresponds to the distribution of coronary arteries shown.

study, the homogeneity index, H, is given by the following equation:

$$H = \sum_m [1/(1 + m)^2] Pd(m). \qquad \text{Eq. 1}$$

The homogeneity index, H, can have values between 0 (noninclusive) and 1 (inclusive). A value near 0 represents an image with a high probability that neighboring pixels have intensity values that differ greatly. The homogeneity index cannot be 0 because at least one Pd(m) must be nonzero. A large value near 1 represents an image with a high probability that neighboring pixels have similar intensity values. In principle, the homogeneity index can be 1, in which case all pixels have the same intensity.

The homogeneity index thus quantifies mathematically the intuitive notion of homogeneity. A perfusion image that is inhomogeneous or diffusely patchy has a small homogeneity index near 0, whereas a uniform image has a large index near 1. Conversely, an image with a small homogeneity index can be considered to be heterogeneous and vice versa. Each pixel can have a maximum of 8 neighbors: above, below, left, right, above left, above right, below left, and below right, where a complete topographic map is like the surface of a cylinder and "wraps" along the radial dimension. There are 5,184 unique pixel pairs for a 21 × 64 matrix, assuming the 64-axis wraps. Intensity of the image matrix is normalized to 1,000. More generally, for an N-by-M matrix, assuming the M-axis wraps, there are (4NM − 3M) unique pixel pairs. Radial pixel size and, hence, heart size does not impact the calculation of the heterogeneity index.

Equation 1 shows that as the differences among neighboring pixel units become larger for severe defects, the coefficient $1/(1 + m)^2$ decreases rapidly with increasing m, corresponding to increasing differences of intensity between neighboring pixels. Expanding the summation in Equation 1 for differences of m = 0, 1, 2, 3, etc., yields the following:

$$\text{Homogeneity Index} = Pd(0) + 1/4\, Pd(1) + 1/9\, Pd(2) + 1/16\, Pd(3) + \ldots$$

This expansion shows that for a difference of 2 between neighboring pixel units, the contribution of the corresponding component, Pd(2), contributes just over 11% as much as Pd(0) to the homogeneity index. Therefore, the homogeneity index, H, expresses as a single number the probability distribution of differences among neighboring pixel units that is weighted for small differences among neighboring pixel units with little influence on H by large differences due to severe discrete regional defects. The value of H therefore objectively quantifies the extent of the mild diffuse heterogeneous patchy pattern on PET images separately from, independent of, and around more severe discrete regional perfusion defects caused by flow-limiting stenosis.

Application of Homogeneity Analysis to PET Perfusion Images. The rest and stress scans are displayed as topographic displays in 4 quadrant views (lateral, inferior, septal, and anterior).

For applying Equation 1 to this topographic map, 3 modifications were made as follows: (i) The basal 4 slices are discarded to avoid count variability in the membranous septum and the apical 2 slices are discarded to minimize partial-volume effects and variability in locating the last apical slice; (ii) pixels with intensity values below 500 are reset to 500, and pixels with intensity values above 850 are reset to 850 to eliminate any effect on the homogeneity index, H, of very low activity levels of myocardium scar and to eliminate effects of the highest activity levels of normal myocardium.

In effect, these limits further confine the homogeneity analysis to relative activity values ranging from 50% to 85% of maximum on each PET image, thereby excluding extreme values as from severe defects or hot spots that would bias the value of H for quantifying more subtle differences among pixel units; (iii) these modified intensity values, 500–850 inclusive, are scaled into an integer range of 35 levels, so that each new intensity level represents 1% of the range, thereby mathematically further restricting the analysis to myocardium that is not scarred, severely ischemic, or maximally perfused. Consequently, the homogeneity index is not greatly influenced by severe perfusion defects. The degree of small-scale diffuse heterogeneous "patchiness" is objectively quantified on resting and stress images and the rest-to-stress change independently of, separately from, or around severe discrete regional perfusion defects due to myocardial scar, reduced coronary flow reserve of flow-limiting stenosis, or the base-to-apex longitudinal perfusion gradient due to diffuse disease (*30*). The scaling impacts the heterogeneity index and determines the "coarseness" or the degree of patchiness being quantified.

Mean and SD values for the homogeneity index, H, were computed for the 50 healthy control subjects just as for the other automated quantitative measurements on the PET images for comparison with the patients in this study.

Statistical Analysis

All statistical analyses were performed using SPSS version 11.5 (SPSS Inc.). Data are reported as mean ± 1 SD or SEM as appropriate.

Analysis 1. Multivariate logistic regression analysis was performed with the independent variables being the continuous values of the resting homogeneity index (rH), the rest-to-stress change in H (rsHΔ), and all discrete risk factors of age, sex, history of diabetes, hypertension, high cholesterol, family history of vascular disease, excess weight, smoking, menopausal status, and lack of exercise. The dependent variables were an abnormal PET after dipyridamole (stress PET) defined as either the lowest mean quadrant activity on the stress PET image, Q, outside 1 SD of healthy reference subjects ($Q < 1$ SD), indicating flow-limiting stenosis, or the base-to-apex longitudinal perfusion gradient (L) after dipyridamole outside 1 SD of healthy reference subjects ($L < 1$ SD), indicating diffuse coronary artery narrowing as previously demonstrated (*30*). An abnormal stress PET therefore includes all cases with any abnormality of either Q or L and excludes those with completely normal Q and L—that is, both $Q > 1$ SD and $L > 1$ SD. It indicates a not-normal PET perfusion scan after dipyridamole stress attributed to either a localized regional defect or an abnormal base-to-apex longitudinal perfusion abnormality outside 1 SD of healthy reference subjects, thereby objectively documenting even mild CAD.

Analysis 2. Multivariate linear regression analysis was performed with the same independent variables as above—that is, the continuous values of the resting homogeneity index (rH), the rest-to-stress change in H (rsHΔ), and all discrete risk factors. The dependent variable is the continuous value of the lowest mean quadrant activity of the stress PET image (Q), indicating the quantitative severity of regional perfusion defects after dipyridamole caused by flow-limiting stenosis.

A Pearson χ^2 analysis was performed for the discrete variables as follows: abnormal homogeneity ($rH < 2$ SD or $rsH\Delta < 2$ SD), borderline homogeneity (rH and rsHΔ within 1–2 SD), normal homogeneity ($rH > 1$ SD and $rsH\Delta > 1$ SD), abnormal stress scans ($Q < 2$ SD or $L < 2$ SD), borderline stress scans (Q and L within 1–2 SD), and normal stress scans ($Q > 1$ SD and $L > 1$ SD). A 2-tailed P value < 0.05 was considered statistically significant.

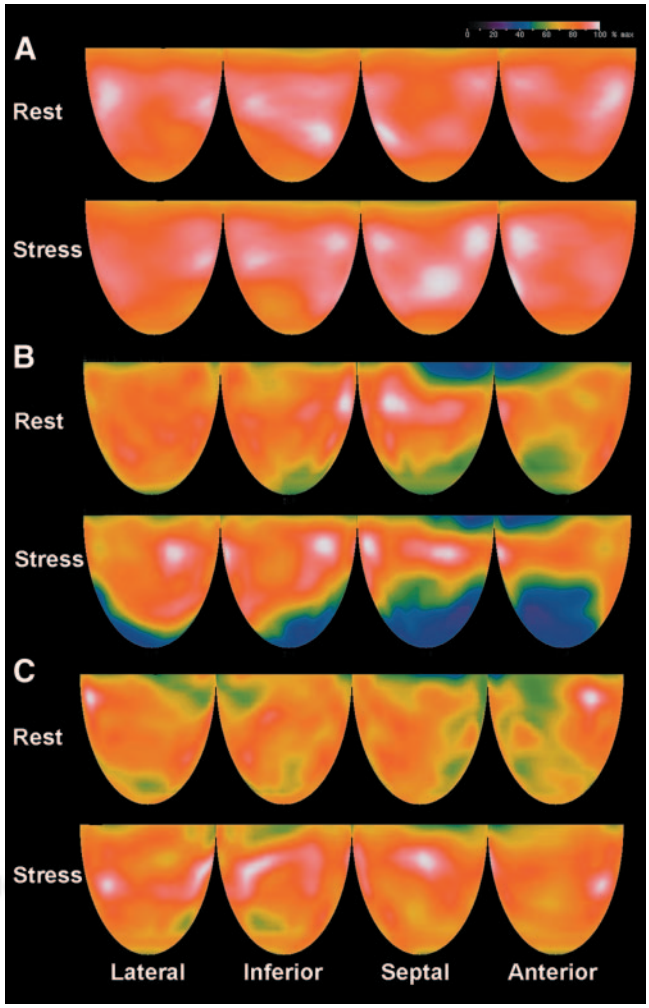

FIGURE 2. PET at rest and after dipyridamole stress in 3 clinical examples. As indicated by the color bar, white indicates maximal relative perfusion; red, high perfusion; yellow, intermediate; green and blue, progressively lower perfusion in continuous graded steps. (A) Young healthy normal volunteer without risk factors for vascular disease. (B) Severe stress-induced perfusion defect. (C) Abnormal base-to-apex longitudinal perfusion gradient with only a mild stress-induced regional perfusion defect.

RESULTS

Complete data on 1,034 patients were analyzed. Figure 1 illustrates orientation of PET perfusion images in lateral, inferior, right, and anterior topographic views. Figure 2 shows 3 examples of rest-dipyridamole PET illustrating the range of images and quantitative measurements of the homogeneity index, the severity of stress-induced regional perfusion defects caused by flow-limiting stenosis, and the base-to-apex longitudinal perfusion gradient due to diffuse coronary atherosclerosis. The first pair of rest–stress images (Fig. 2A) are of a young healthy volunteer with no coronary risk factors as an example of normal perfusion images. The second rest–stress pair (Fig. 2B) is from a patient with a severe stress-induced perfusion defect in the distribution of the mid left anterior descending coronary artery. This example of a severe stress-induced perfusion defect illustrates that the Markovian homogeneity analysis is independent of and separate from even severe perfusion defects because it improves from a low value of 0.34 at rest that is < 2 SD of the healthy reference group to 0.49 after dipyridamole, within 1 SD of normal, despite a severe stress-induced perfusion defect. The third rest–stress pair (Fig. 2C) is from a patient with an abnormal base-to-apex longitudinal perfusion gradient due to diffuse CAD without severe localized flow-limiting stenosis (confirmed by coronary arteriography).

Figure 3 shows the corresponding graphic displays of homogeneity analysis for these same 3 examples in the same order. For the first rest–stress pair (Fig. 3A), the homogeneity index by Markovian analysis is 0.80 at resting conditions and remains comparable at 0.83 after dipyridamole, both within the normal limits of 50 healthy con-

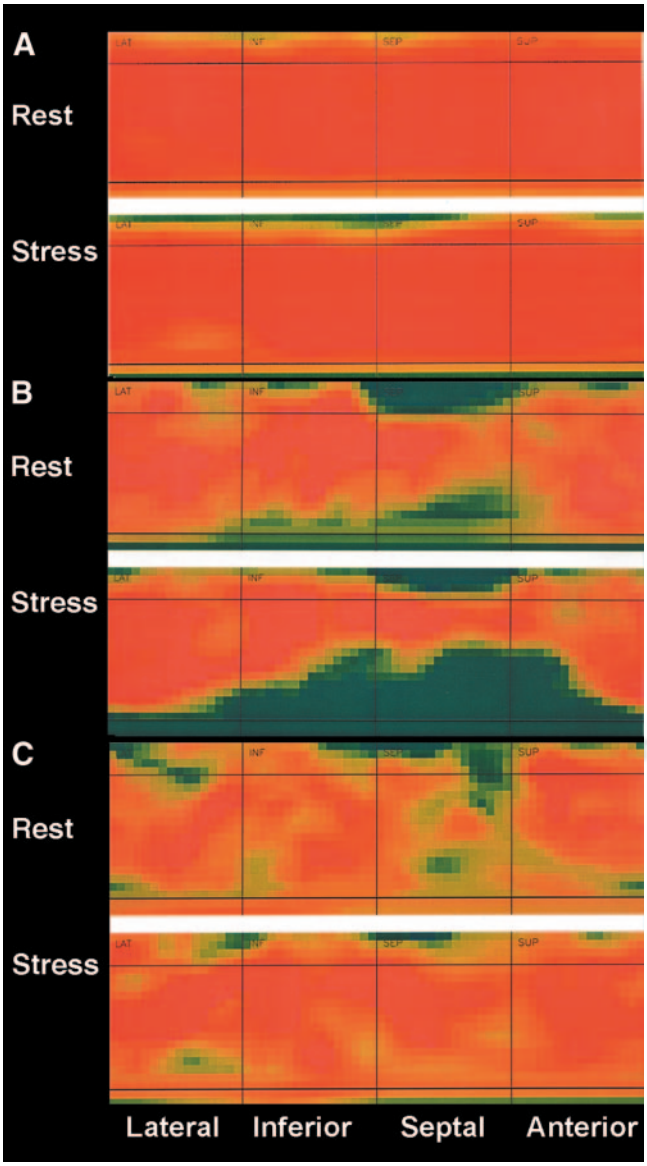

FIGURE 3. Display of relative activity distribution for Markovian homogeneity analysis, where each square panel corresponds to quadrants of the same 3 people illustrated in Figures 1 and 2. Quadrant squares indicate the area of heterogeneity analysis with the basal 4 slices and apex excluded from analysis as described. For the first rest–stress pair of the healthy control person (A), resting homogeneity index is 0.80 at rest and 0.83 after dipyridamole, both within normal limits of 50 healthy control subjects. For the second rest–stress pair of the person with a severe stress-induced perfusion defect (B), the homogeneity index is 0.34 at rest that is $<$ 2 SD of healthy reference subjects and improves to 0.49 after dipyridamole, within 1 SD of healthy reference subjects, despite a severe stress-induced perfusion defect. For the third rest–stress pair of the person with a minimal perfusion abnormality (C), the homogeneity index is 0.26 at rest and improves to 0.40 after dipyridamole with an abnormal base-to-apex longitudinal perfusion gradient but no severe regional stress-induced perfusion defect.

trol subjects. The second rest–stress pair (Fig. 3B) shows severe resting perfusion heterogeneity with a homogeneity index of 0.34 that is $<$ 2 SD of healthy reference subjects and improves after dipyridamole to 0.49, within 1 SD of healthy reference subjects, in regions around the severe stress-induced perfusion defect due to flow-limiting coronary artery stenosis. As a quantitative measure of the stress-induced perfusion defect, the lowest mean average quadrant activity on the dipyridamole scan is 63% of maximum that is $<$ 7 SD of healthy reference subjects and the base-to-apex longitudinal perfusion gradient is $<$ 5 SD of normal limits. This example illustrates that the homogeneity index quantifies the patchy heterogeneous perfusion pattern separately from, independently of, and around localized regional perfusion defects.

The third rest–stress pair (Fig. 3C) illustrates severe resting perfusion heterogeneity with a resting homogeneity index of 0.26 that improves after dipyridamole to 0.40 without a severe stress-induced perfusion defect but with a markedly abnormal base-to-apex longitudinal perfusion gradient that is 2.6 SD units away from healthy reference subjects. Although the regional stress-induced defect is not as severe as in the prior example, 10% of the image had activity that was also $<$ 2.5 SD of normal reference subjects. For the 50 healthy reference subjects, the mean homogeneity index is 0.63 $\pm$ 0.13 at rest and 0.69 $\pm$ 0.11 after dipyridamole, a significant difference ($P < 0.001$).

Figure 4 illustrates the base-to-apex longitudinal perfusion gradient of these same 3 pairs of rest–stress PET scans, being within normal limits for the first pair (Fig. 4A) and markedly abnormal for the other 2 examples (Figs. 4B and 4C), indicating diffuse CAD plus a severe localized flow-limiting stenosis (Fig. 4B) or without a severe localized flow-limiting stenosis (Fig. 4C).

Table 1 summarizes the logistic regression analysis for the resting homogeneity index (H), its rest-to-stress improvement (rsHΔ), and the risk factors as the independent variables. The discrete dependent variable is any abnormality of the stress perfusion scan, either the minimum quadrant average activity outside, or greater than, Q $>$ 1 SD of healthy reference subjects or the base-to-apex longitudinal perfusion gradient outside, or greater than, L $>$ 1 SD of healthy reference subjects on stress PET images. As expected, standard risk factors are predictive of abnormal stress perfusion images. A family history of vascular disease and smoking were not significantly predictive because of the brevity of details of the history recorded in the database options. The family history did not differentiate among parents, siblings, or remote relations. Smoking did not differentiate among remote brief smoking, active current smoking, or amount of smoking.

The resting homogeneity index and its rest-to-stress change are powerful predictors of stress-induced perfusion abnormalities separately from and independently of standard risk factors. The much larger values of B in the regression equation indicate that resting heterogeneity and

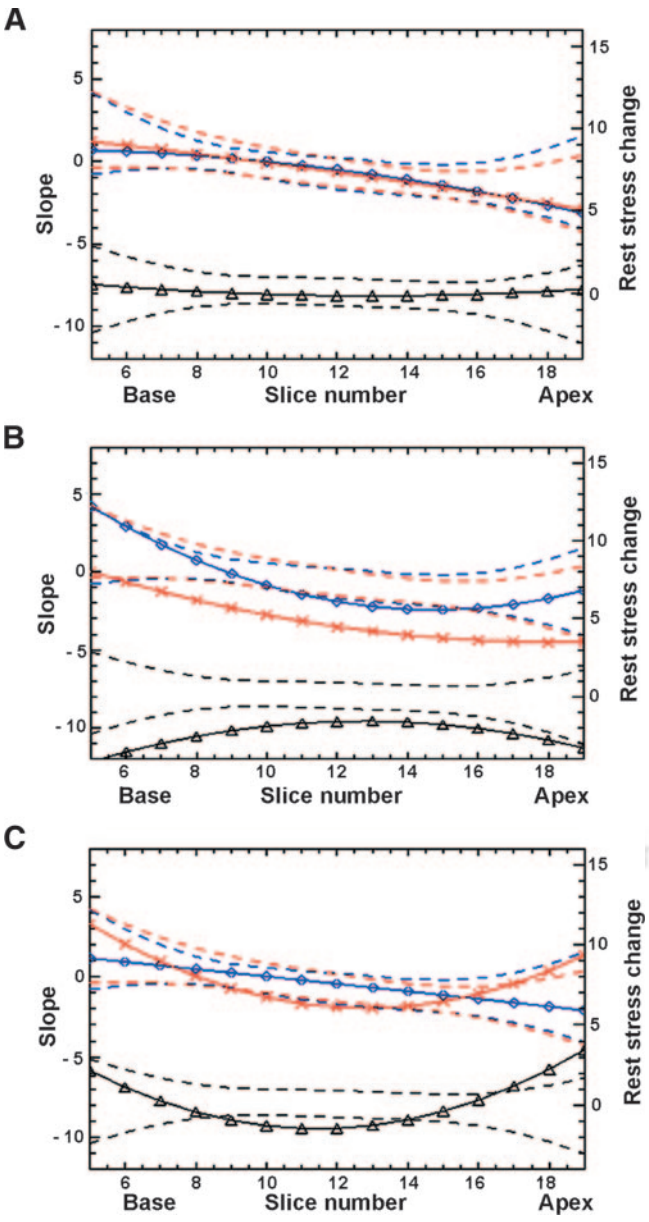

FIGURE 4. Graphs of base-to-apex longitudinal perfusion gradient expressed as first derivative or spatial slope of relative activity (vertical axis) at each tomographic slice from base-to-apex (horizontal axis) at rest (blue diamonds) and with dipyridamole stress (red Xs) with +2 SD and –2 SD limits of 50 reference subjects at rest (blue dashes) and after diypridamole (red dashes) for the same 3 clinical examples illustrated in Figures 2 and 3. Slope units are changes in relative activity per slice from base to apex. For the healthy control person (A), the base-to-apex longitudinal perfusion gradient at rest and during dipyridamole stress and the rest-to-stress change are both within 2 SD of 50 healthy control subjects. For the person with the severe stress-induced perfusion defect (B), the longitudinal perfusion gradient at rest and stress and the rest-to-stress change are all outside 2 SD of healthy reference subjects. For the person with the minimal perfusion abnormality (C), the longitudinal perfusion gradient and its rest-to-stress change are outside 2 SD limits of healthy reference subjects even though there is no clinically significant localized regional stress-induced perfusion defect.

its rest-to-stress improvement are not only independent of but also markedly more powerful predictors of stress-induced myocardial perfusion abnormalities than standard risk factors.

The negative values of B for the homogeneity index (rH) and its rest-to-stress change (rsHΔ) indicate that high values of rH or rsHΔ are associated with very high probability of normal stress perfusion images (the minimum quadrant average activity Q less than or within 1 SD of healthy reference subjects) and a low probability of abnormal stress perfusion images (Q greater than or outside 1 SD of healthy reference subjects). Similarly, low values of rH or its rest-to-stress change, rsHΔ, are associated with a very high probability of abnormal stress perfusion defects ($Q > 1$ SD) and a low probability of normal stress perfusion images ($Q < 1$ SD).

For logistic regression, which uses a sigmoid/logistic model instead of a linear one, B is the logarithm of the odds ratio, and EXP(B) is the ratio of the odds—that is, the probability of something occurring divided by the probability of something not occurring, quantified as EXP(B). For example, in this analysis for diabetes, B is 1.64, the EXP(B) is $e^{1.64}$ or 5.15,—that is, the odds ratio for diabetes. Therefore, a person with a history of diabetes carries a 5.15 times greater odds of an abnormal stress PET scan than the odds for a person without a history of diabetes.

For the homogeneity index, B is −23.05, the EXP(B) is $e^{-23.05}$ or 1.03×10^{-10}—that is, the odds ratio for the homogeneity index. Therefore, the odds of a patient with a normal homogeneity index (HI = 1.0) having an abnormal stress PET scan is only 0.000000000103 of the odds for a patient with an abnormal homogeneity index (HI = 0.0+) of having an abnormal stress PET. Similarly, the odds for a patient with an abnormal homogeneity index of having a normal stress image is an equally small percent of the odds for a patient with a normal homogeneity index of having a normal stress image. From the other viewpoint, the odds for a person with an abnormal resting homogeneity index (HI = 0.0+) of having an abnormal stress PET is 1/0.0000000103 or 9.7×10^9 times the odds of a person with a normal homogeneity index (HI + 1.0) of having an abnormal stress PET. Separately and independently of the resting homogeneity index, rH, the rest-to-stress improvement in the homogeneity index, rsHΔ, after dipyridamole stress is comparably predictive of CAD with a comparable odds ratio.

Table 2 summarizes the multivariate linear regression analysis with the independent variables being the resting perfusion homogeneity index (rH), the rest–stress change in homogeneity index (rsHΔ), and all risk factors together in the first 5 rows and for the risk factor alone without the PET data in rows 7 through 17. The single dependent variable is the continuous quantitative severity of stress perfusion defects—that is, the minimum average quadrant activity on the stress PET images (Q). This analysis shows that the resting homogeneity index and its rest-to-stress improvement are closely correlated with stress-induced regional

TABLE 1
Multivariate Stepwise Logistic Regression Analysis for Any Stress-Induced Myocardial Perfusion Abnormality by PET as the Dependent Variable

Independent variable	Dependent variable: discrete, any abnormality	B	EXP(B)	95% CI of EXP(B)	*P* for significance
Resting homogeneity index, rH	Q < 1 SD or L < 1 SD	−23.1	0.000	0.000–0.000	<0.001
Rest-to-stress change in H, rsHΔ	Q < 1 SD or L < 1 SD	−22.2	0.000	0.000–0.000	<0.001
Male	Q < 1 SD or L < 1 SD	1.99	7.29	3.40–15.63	<0.001
Age	Q < 1 SD or L < 1 SD	0.02	1.02	1.00–1.04	0.019
Hx of diabetes	Q < 1 SD or L < 1 SD	1.88	6.57	2.39–18.03	<0.001
Hx of hypertension	Q < 1 SD or L < 1 SD	0.55	1.73	1.29–2.33	<0.001
Hx of overweight	Q < 1 SD or L < 1 SD	0.43	1.53	1.13–2.07	<0.001
Hx of exercise	Q < 1 SD or L < 1 SD	0.57	1.77	1.04–3.02	0.036
Hx of high cholesterol	Q < 2 SD	0.85	2.33	1.32–4.11	0.004
Postmenopausal	Q < 2 SD	3.02	20.45	1.98–288.2	0.011
Family Hx of vascular disease	Q < 2 SD	−0.18	0.84	0.48–1.47	NS
Hx of smoking	Q < 2 SD	0.06	1.07	0.78–1.45	NS

B = $\log_e$ of odds ratio; EXP = exponent; Q = lowest average quadrant activity on stress PET image; L = longitudinal base-to-apex perfusion gradient on stress PET image; Hx = history; NS = not significant.

perfusion defects separately from and independently of other risk factors ($P < 0.001$). For linear regression analysis of continuous variables, B is the "slope" of the regression equation (coefficient of the independent variable in the fitted equation) that is substantially greater for the resting homogeneity index and its rest-to-stress change than for any of the standard risk factors.

The negative values of B for the risk factors indicate that the standard risk factors are associated with more severe stress-induced perfusion abnormalities—that is, lower values of the minimum quadrant average activity, Q. The positive values of B for homogeneity index (H) and its rest-to-stress change indicate that low values of rH—that is, more heterogeneous resting perfusion images are associated with more severe stress-induced perfusion abnormalities—that is, lower values of the minimum average quadrant activity, Q. Similarly high values of rH are associated with less severe stress-induced perfusion abnormalities or normal images—that is, high values of Q. For linear regression, the odds ratios based on B are not applicable. Quantitative severity of the stress perfusion defects, Q, was not predicted by family history of vascular disease, smoking, postmenopausal status, or history of high cholesterol—again, most likely due to the brevity of the history details that also did not account for cholesterol levels or its treatment.

TABLE 2
Multivariate Stepwise Linear Regression Analysis for Severity of Stress-Induced Myocardial Perfusion Abnormality as the Continuous Dependent Variable (Q)

Independent variable, all risk factors and PET images	B	*P* for significance
Resting homogeneity index, rH	38.0	<0.001
Rest-to-stress change in H, rsHΔ	34.3	<0.001
Hx of diabetes	−3.31	<0.001
Age	−0.07	<0.001
Independent variable: risk factors only		
Male	−5.71	<0.001
Age	−0.11	<0.001
Hx of diabetes	−4.74	<0.001
Hx of overweight	−1.86	0.001
Hx of hypertension	−1.34	0.016
Hx of smoking	−1.13	0.033
Family Hx of vascular disease	0.49	NS
Postmenopausal	−0.75	NS
Hx of exercise	−0.48	NS
Hx of high cholesterol	−1.11	NS

Q = lowest average quadrant activity on stress PET; B = slope of linear regression; Hx = history; NS = not significant.

Table 3 shows the χ^2 analysis with numbers of subjects in each category where homogeneity was defined as "abnormal" if either the resting homogeneity index or its rest-to-stress improvement were outside or < 2 SD of healthy reference subjects, "normal" if both were >2 SD, and "borderline" for all other combinations of the rest and rest-to-stress change as mixed 1–2 SD, < 2 SD, and > 2 SD. Similarly, stress images were defined as "abnormal" if either the lowest mean quadrant average activity (Q) caused by flow-limiting stenosis or the longitudinal base-to-apex perfusion gradient (L) due to diffuse CAD were < 2 SD of healthy reference subjects, normal if both were > 2 SD, and borderline for all other combinations. In Table 3, the distribution of subjects in the binary discrete categories of homogeneity and stress perfusion categories is significant with $P < 0.001$. Table 4 shows the relative or percentage distribution of the χ^2 distribution of raw numbers in Table 3 expressed in Table 4 as the percentage of the patients in each homogeneity category in rows from left to right across the table. Figure 5 is a bar graph of the relative percentage

TABLE 3
Number of Patients in χ^2 Analysis

	Stress abnormal (*n*)	Stress borderline (*n*)	Stress normal (*n*)	Total (*n*)
Homogeneity abnormal	171	22	16	209
Homogeneity borderline	316	90	127	533
Homogeneity normal	72	38	182	292
Total	559	150	325	1,034

Homogeneity was defined as "abnormal" if the resting homogeneity index and its rest-to-stress change were both $<$ 2 SD of healthy reference subjects, "normal" if both were $>$ 2 SD, and "borderline" for all other unequal combinations of rest and rest-to-stress change as 1–2 SD, $<$ 2 SD, and $>$ 2 SD.

distribution of patients in each of the homogeneity categories derived from the χ^2 analysis in Table 3 and the percentage distributions in Table 4.

Table 5 shows the mean values of the homogeneity index (rH), the severity of the stress perfusion defect (Q) and the longitudinal perfusion gradient (L) for all patients grouped according to a binary classification based on the homogeneity index being $>$ 2 SD, 1–2 SD, $<$ 1 SD for comparison with the mean values for the healthy control subjects. Mean values in all the categories are significantly different from healthy control subjects with $P < 0.001$ and are different from each other by ANOVA with $P < 0.001$.

DISCUSSION

Coronary endothelial dysfunction refers to a wide spectrum of coronary vasomotor pathophysiology associated with preclinical and clinical CAD that may involve epicardial arteries or microvasculature, different vasoactive mediators, different stimuli, and different pathophysiologic or clinical manifestations. However, assessing coronary endothelial dysfunction and application of extensive research knowledge have not been clinically developed because of its complexity and lack of noninvasive approaches. This study reports a new concept in perfusion imaging by demonstrating a close relation between resting perfusion heterogeneity outside normal limits with early or advanced coronary disease in a large number of patients with well-defined risk factors based on the association of endothelial dysfunction with microvascular dysfunction.

Endothelial dysfunction as a cause of coronary arterial and microvascular vasoconstriction is well documented in experimental studies and in humans by coronary arteriography or Doppler flow-velocity wires or catheters. Vascular mediators derived from coronary endothelium include prostacyclin, nitric oxide, thromboxane, endothelin, bradykinin, angiotensin, serotonin, substance P, C-type naturetic peptide ([CNP], an endothelium-derived hyperpolarizing factor), and others. The mechanisms may be inhibition of normal vasodilatory mediators such as nitric oxide or activation of vasoconstrictor mediators such as endothelin.

The stimuli, mediators, and the vascular responses of epicardial coronary arteries and the coronary microvasculature are quite different, even divergent. For example, in the epicardial coronary arteries, acetylcholine-induced vasodilation is mediated by nitric oxide (*20,35,36*). However, in the coronary microcirculation, acetylcholine-induced arteriolar vasodilation and increased coronary flow are not mediated by nitric oxide (*18,37,38*). With epicardial artery endothelial dysfunction, acetylcholine causes arterial vasoconstriction while arteriolar vasodilation with increased flow remains intact as an example of divergent pathophysiologic behavior of the macrovasculature and microvasculature of the heart (*18–22*).

As a further example, endothelial nitric oxide production mediates epicardial coronary artery vasodilation during exercise (*19*) but is not involved in arteriolar vasodilation and increased coronary flow during exercise (*19*) unless there is a flow-limiting stenosis in which nitric oxide helps maintain perfusion during exercise (*39*). In opposition to these vasodilator mechanisms, endothelin is a powerful coronary arteriolar vasoconstrictor that is activated in coronary atherosclerosis in parallel with inhibition of nitric oxide production.

Thus, there is no single specific vasomotor abnormality, gold standard, diagnostic test, or even definition that identifies or defines coronary endothelial dysfunction. Our data indicate that resting myocardial perfusion heterogeneity is one manifestation of this wide spectrum of coronary vascu-

TABLE 4
Percentage Distribution of Patients in Each Homogeneity Group

	Stress abnormal (%)	Stress borderline (%)	Stress normal (%)	*n*	%
Homogeneity abnormal	82	11	8	209	100
Homogeneity borderline	59	17	24	533	100
Homogeneity normal	25	13	62	292	100

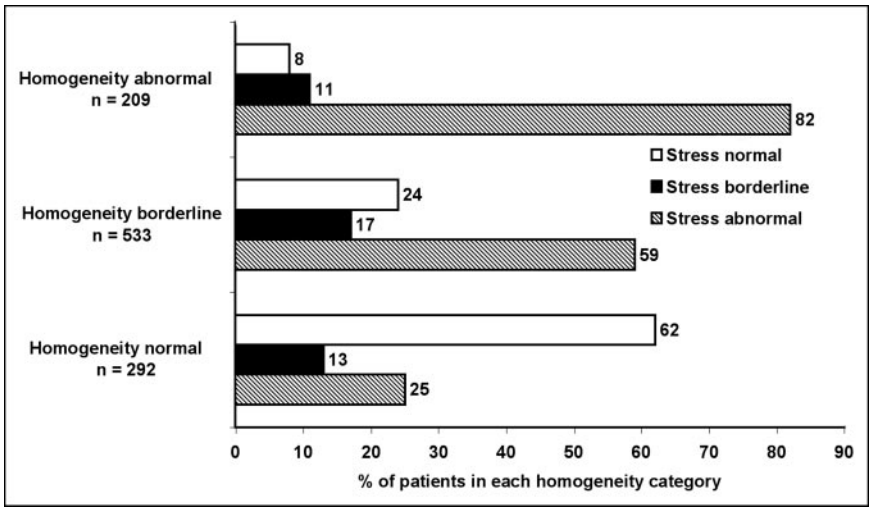

FIGURE 5. Bar graph of relative percentage distribution of subjects in χ^2 relative distribution of Table 3. Homogeneity was defined as abnormal if the resting homogeneity index and its rest-to-stress change were $<$ 2 SD of healthy reference subjects, normal if both were $>$ 2 SD, and borderline for all other unequal combinations of rest and rest-to-stress change as 1–2 SD, $<$ 2 SD, and $>$ 2 SD.

lar behavior that is a powerful independent predictor of preclinical CAD, more than standard risk factors. In view of the different, sometimes divergent, arterial and arteriolar behaviors in response to the wide variety of vasoactive mediators, resting perfusion heterogeneity would not necessarily be expected to parallel the effects of intracoronary acetylcholine or cold pressor testing, just as the arteriolar response to acetylcholine with increased blood flow does not parallel its vasoconstrictive effect on epicardial coronary arteries in CAD.

The limitations of this study deserve comment. A criticism may be that the limited resolution of PET cannot resolve the small regions of heterogeneous perfusion previously described in experimental animals (*40*) or the subendocardial underperfusion that is an effect of flow-limiting stenosis. The heterogeneity that is visually apparent and objectively quantified in this study involves regions of myocardium greater than the 1-cm^3 scanner resolution, consistent with the arterial distribution of coronary arteries and their secondary or tertiary branches demonstrated to have heterogeneous endothelial function by coronary arteriography and intracoronary Doppler flow-velocity measurements. Therefore, the heterogeneity that we observe by PET perfusion imaging is separate and unrelated to the dispersion of perfusion in small 1-mm myocardial samples for microsphere measurements of perfusion reported for experimental animals (*40*).

The heterogeneous resting perfusion in this study was quantified separately from, independently of, and around significant regional perfusion defects caused by flow-limiting stenosis and, therefore, does not involve subendocardial hypoperfusion due to reduced perfusion pressure or reduced early diastolic subendocardial filling caused by flow-limiting stenosis.

The limits of heterogeneity were determined from 50 healthy control subjects imaged on the same scanner and software as the patients so that the technical limitations of PET or any potential effects of microscopic dispersion apply equally to both sets of subjects with the significant differences reported here. The application of homogeneity analysis to PET perfusion images requires careful attention to the technical details of cardiac PET with ^{82}Rb that are different than those required for cancer PET, including the necessity of lower spatial resolution in favor of a high count density, 2D imaging to reduce scattered radiation, high-count, low-noise, filtered backprojection reconstruction, and compulsive correction of emission–transmission image coregistration (*34*).

Coronary arteriography was not performed or used as a comparative gold standard in all of these patients. The

TABLE 5
Mean Values of Quantitative Endpoints

Binary rH group	Resting homogeneity index, rH	Q	L	*n*
$<$ 2 SD	0.32 ± 0.036*	70.9 ± 9.1*	1.61 ± 1.85*	157
1–2 SD	0.44 ± 0.035*	73.3 ± 9.6*	0.85 ± 1.44*	388
$>$ 1 SD	0.61 ± 0.079*	77.6 ± 7.4*	0.66 ± 1.24*	439
Healthy reference subjects	0.63 ± 0.127	82.3 ± 2.8	0.09 ± 0.45	50

*$P < 0.001$ compared with healthy reference subjects and for ANOVA for differences between the 3 patient groups.
Q = lowest average quadrant activity on stress PET image, % of maximum activity in whole heart dataset; L = longitudinal base-to-apex perfusion gradient on stress PET image in SD units.

percentage diameter stenosis as a measure of the severity of CAD is notoriously inadequate because of diffuse disease. The base-to-apex longitudinal perfusion gradient by PET perfusion imaging identifies early diffuse CAD better than regional stress-induced perfusion defects of flow-limiting stenosis as we have demonstrated (*30*). Because coronary atherosclerosis is a continuous spectrum from early mild stages to severe stenosis, the conventional categorization of arteriograms or perfusion images into "normal" or "abnormal" for determination of sensitivity or specificity is artificial and incorrect, particularly when defined as outside 2 SD of normal. Our multivariate regression analysis using continuous quantitative variables confirms the continuous spectrum of these endpoints. Accordingly, for added certainty, we performed logistic regression analysis using as thresholds of our endpoints a cutoff of < 1 SD as "not normal"—that is, a greater probability of being "abnormal" than "normal" to include the great extent of mild preclinical CAD with potential for plaque rupture and coronary events.

Although resting perfusion heterogeneity or its improvement is associated with "not normal" stress perfusion PET scans, some patients with resting perfusion heterogeneity had normal stress perfusion PET scans. By association with otherwise comparable patients with stress-induced perfusion changes, our findings suggest that such patients with heterogeneity or its improvement without stress-induced defects are at risk for vascular disease. However, our data do not prove that point. Proof would require many years' follow-up of such patients off lipid medications to determine the outcomes, a difficult study that is not ethically appropriate.

CONCLUSION

Patchy diffuse heterogeneity of resting myocardial perfusion by noninvasive PET quantified objectively by automated software using Markovian mathematic analysis is a powerful independent predictor of even mild stress-induced perfusion defects or base-to-apex longitudinal perfusion gradients of diffuse CAD and is more predictive than standard risk factors, consistent with coronary microvascular dysfunction-associated early or advanced CAD for potential preventive treatment.

ACKNOWLEDGMENTS

This research was supported in part by The Weatherhead Foundation Endowment, the Martin Bucksbaum Distinguished University Chair, and an American Medical Foundation Seed Grant.

REFERENCES

1. Verma S, Anderson TJ. Fundamentals of endothelial function for the clinical cardiologist. *Circulation.* 2002;105:546–549.
2. Clarkson P, Celermajer DS, Powe AJ, Donald AE, Henry RM, Deanfield JE. Endothelium-dependent dilatation is impaired in young healthy subjects with a family history of premature coronary disease. *Circulation.* 1997;96:3378–3383.
3. Suwaidi JA, Hamasaki S, Higano ST, Nishimura RA, Holmes DRJ, Lerman A. Long-term follow-up of patients with mild coronary artery disease and endothelial dysfunction. *Circulation.* 2000;101:948–954.
4. Schachinger V, Britten MB, Zeiher AM. Prognostic impact of coronary vasodilator dysfunction on adverse long-term outcome of coronary heart disease. *Circulation.* 2000;101:1899–1906.
5. Halcox JP, Schenke WH, Zalos G, et al. Prognostic value of coronary vascular endothelial dysfunction. *Circulation.* 2002;106:653–658.
6. Bugiardini R, Manfrini O, Pizzi C, Fontana F, Morgagni G. Endothelial function predicts future development of coronary artery disease: a study of women with chest pain and normal coronary angiograms. *Circulation.* 2004;109:2518–2523.
7. Bottcher M, Madsen MM, Refsgaard J, et al. Peripheral flow response to transient arterial forearm occlusion does not reflect myocardial perfusion reserve. *Circulation.* 2001;103:1109–1114.
8. Nesto RW, Lamas GA, Barry J. Paradoxical elevation of threshold to angina pectoris by cold pressor test in men with significant coronary artery disease. *Am J Cardiol.* 1989;63:656–659.
9. Kjaer A, Meyer C, Nielsen FS, Parving HH, Hesse B. Dipyridamole, cold pressor test, and demonstration of endothelial dysfunction: a PET study of myocardial perfusion in diabetes. *J Nucl Med.* 2003;44:19–23.
10. el-Tamimi H, Mansour M, Wargovich TJ, et al. Constrictor and dilator responses to intracoronary acetylcholine in adjacent segments of the same coronary artery in patients with coronary artery disease: endothelial function revisited. *Circulation.* 1994;89:45–51.
11. Penny WF, Rockman H, Long J, et al. Heterogeneity of vasomotor response to acetylcholine along the human coronary artery. *J Am Coll Cardiol.* 1995;25:1046–1055.
12. Kuo L, Davis MJ, Chilian WM. Longitudinal gradients for endothelium-dependent and -independent vascular responses in the coronary microcirculation. *Circulation.* 1995;92:518–525.
13. Chilian WM, Dellsperger KC, Layne SM, et al. Effects of atherosclerosis on the coronary microcirculation. *Am J Physiol.* 1990;258:H529–H539.
14. Sellke FW, Armstrong ML, Harrison DG. Endothelium-dependent vascular relaxation is abnormal in the coronary microcirculation of atherosclerotic primates. *Circulation.* 1990;81:1586–1593.
15. Kuo L, Davis MJ, Cannon MS, Chilian WM. Pathophysiological consequences of atherosclerosis extend into the coronary microcirculation: restoration of endothelium-dependent responses by L-arginine. *Circ Res.* 1992;70:465–476.
16. Zeiher AM, Drexler H, Wollschlager H, Just H. Endothelial dysfunction of the coronary microvasculature is associated with coronary blood flow regulation in patients with early atherosclerosis. *Circulation.* 1991;84:1984–1992.
17. Zeiher AM, Drexler H, Wollschlager H, Just H. Modulation of coronary vasomotor tone in humans: progressive endothelial dysfunction with different early stages of coronary atherosclerosis. *Circulation.* 1991;83:391–401.
18. Shiode N, Morishima N, Nakayama K, Yamagata T, Matsuura H, Kajiyama G. Flow-mediated vasodilation of human epicardial coronary arteries: effect of inhibition of nitric oxide synthesis. *J Am Coll Cardiol.* 1996;27:304–310.
19. Loscalzo J, Vita JA. Ischemia, hyperemia, exercise, and nitric oxide: complex physiology and complex molecular adaptations. *Circulation.* 1994;90:2556–2559.
20. Quyyumi AA, Dakak N, Andrews NP, et al. Nitric oxide activity in the human coronary circulation: impact of risk factors for coronary atherosclerosis. *J Clin Invest.* 1995;95:1747–1755.
21. Cohen RA, Vanhoutte PM. Endothelium-dependent hyperpolarization: beyond nitric oxide and cyclic GMP. *Circulation.* 1995;92:3337–3349.
22. Schachinger V, Zeiher AM. Quantitative assessment of coronary vasoreactivity in humans in vivo: importance of baseline vasomotor tone in atherosclerosis. *Circulation.* 1995;92:2087–2094.
23. Gould KL. *Coronary Artery Stenosis and Reversing Atherosclerosis*. 2nd ed. London, U.K.: Arnold Publishers; 1999:289–327.
24. Gould KL, Lipscomb K, Hamilton GW. Physiologic basis for assessing critical coronary stenosis: instantaneous flow response and regional distribution during coronary hyperemia as measures of coronary flow reserve. *Am J Cardiol.* 1974;33:87–94.
25. Gould KL. Noninvasive assessment of coronary stenoses by myocardial perfusion imaging during pharmacologic coronary vasodilatation. I. Physiologic basis and experimental validation. *Am J Cardiol.* 1978;41:267–278.
26. Gould KL, Schelbert HR, Phelps ME, Hoffman EJ. Noninvasive assessment of coronary stenoses with myocardial perfusion imaging during pharmacologic coronary vasodilatation. V. Detection of 47 percent diameter coronary stenosis with intravenous nitrogen-13 ammonia and emission-computed tomography in intact dogs. *Am J Cardiol.* 1979;43:200–208.
27. Gould KL, Goldstein RA, Mullani NA, et al. Noninvasive assessment of coronary stenoses by myocardial perfusion imaging during pharmacologic coronary vaso-

dilation. VIII. Clinical feasibility of positron cardiac imaging without a cyclotron using generator-produced rubidium-82. *J Am Coll Cardiol.* 1986;7:775–789.
28. Doudkine A, Macaulay C, Poulin N, Palcic B. Nuclear texture measurements in image cytometry. *Pathologica.* 1995;87:286–299.
29. Demer LL, Gould KL, Goldstein RA, et al. Assessment of coronary artery disease severity by positron emission tomography: comparison with quantitative arteriography in 193 patients. *Circulation.* 1989;79:825–835.
30. Gould KL, Nakagawa Y, Nakagawa K, et al. Frequency and clinical implications of fluid dynamically significant diffuse coronary artery disease manifest as graded, longitudinal, base-to-apex myocardial perfusion abnormalities by noninvasive positron emission tomography. *Circulation.* 2000;101:1931–1939.
31. Sdringola S, Patel D, Gould KL. High prevalence of myocardial perfusion abnormalities on positron emission tomography in asymptomatic persons with a parent or sibling with coronary artery disease. *Circulation.* 2001;103:496–501.
32. Nakagawa Y, Nakagawa K, Sdringola S, Mullani N, Gould KL. A precise, three-dimensional atlas of myocardial perfusion correlated with coronary arteriographic anatomy. *J Nucl Cardiol.* 2001;8:580–590.
33. Sdringola S, Nakagawa K, Nakagawa Y, et al. Combined intense lifestyle and pharmacologic lipid treatment further reduce coronary events and myocardial perfusion abnormalities compared with usual-care cholesterol-lowering drugs in coronary artery disease. *J Am Coll Cardiol.* 2003;41:263–272.
34. Catalin L, Sdringola S, Gould KL. Common artifacts in PET myocardial perfusion images due to attenuation-emission misregistration: clinical significance, causes and solutions. *J Nucl Med.* 2004;45:1029–1039.
35. Casino PR, Kilcoyne CM, Quyyumi AA, Hoeg JM, Panza JA. The role of nitric oxide in endothelium-dependent vasodilation of hypercholesterolemic patients. *Circulation.* 1993;88:2541–2547.
36. Anderson TJ, Meredith IT, Ganz P, Selwyn AP, Yeung AC. Nitric oxide and nitrovasodilators: similarities, differences and potential interactions. *J Am Coll Cardiol.* 1994;24:555–566.
37. Lefroy DC, Crake T, Uren NG, Davies GJ, Maseri A. Effect of inhibition of nitric oxide synthesis on epicardial coronary artery caliber and coronary blood flow in humans. *Circulation.* 1993;88:43–54.
38. Sudhir K, MacGregor JS, Amidon TM, Gupta M, Yock PG, Chatterjee K. Differential contribution of nitric oxide to regulation of vascular tone in coronary conductance and resistance arteries: intravascular ultrasound studies. *Am Heart J.* 1994;127:858–865.
39. Kitakaze M, Node K, Minamino T, et al. Role of nitric oxide in regulation of coronary blood flow during myocardial ischemia in dogs. *J Am Coll Cardiol.* 1996;27:1804–1812.
40. Loncar R, Flesche CW, Deussen A. Coronary reserve of high- and low-flow regions in the dog heart left ventricle. *Circulation.* 1998;98:262–270.